



Efficient synthesis of orthorhombic lithium borate hydroxide micro-rods and their thermal conversion to lithium borate

Wancheng Zhu^{a,*}, Liyun Zhang^a, Xili Cui^a, Qiang Zhang^{b,*}

^a Department of Chemical Engineering, Qufu Normal University, Shandong 273165, China

^b Department of Chemical Engineering, Tsinghua University, Beijing 100084, China

ARTICLE INFO

Article history:

Received 9 October 2010

Received in revised form 26 January 2011

Accepted 26 February 2011

Available online 4 March 2011

Keywords:

Lithium borate

Hydrothermal

Crystal growth

Thermal decomposition

ABSTRACT

Uniform orthorhombic $\text{Li}_3\text{B}_5\text{O}_8(\text{OH})_2$ micro-rods were hydrothermally synthesized at 150–210 °C for 6.0–24.0 h, using $\text{LiOH} \cdot \text{H}_2\text{O}$ and H_3BO_3 as the reactants. The resulting $\text{Li}_3\text{B}_5\text{O}_8(\text{OH})_2$ micro-rods had a length of 20–60 μm , an aspect ratio of 6–14, and a high crystallinity. The presence of hexadecyl trimethyl ammonium bromide was favorable for the oriented growth of the $\text{Li}_3\text{B}_5\text{O}_8(\text{OH})_2$ micro-rods. The orthorhombic $\text{Li}_3\text{B}_5\text{O}_8(\text{OH})_2$ was decomposed into $\text{Li}_2\text{B}_4\text{O}_7$ and $\alpha\text{-LiBO}_2$. Pore-free high crystallinity $\text{Li}_2\text{B}_4\text{O}_7$ with quasi polyhedron morphology can be obtained by NaCl assisted calcination. This enlarged the controllable synthesis of the alkali borates, especially enriched the study on the lithium borates which can be potentially used as a perspective superionic conductor and electrode of lithium ion batteries.

© 2011 Elsevier B.V. All rights reserved.

1. Introduction

Alkali borates, such as $\text{CsLiB}_6\text{O}_{10}$, $\text{KB}_5\text{O}_8 \cdot 4\text{H}_2\text{O}$, CaBeB_2O_5 , LiB_3O_5 , and $\text{Li}_3\text{B}_5\text{O}_8(\text{OH})_2$, have attracted more and more attention owing to their wide range of physical and chemical properties, such as nonlinear optical property and good ionic conductivity [1–8]. Recently, Li-ion batteries are one of the great successes of modern material chemistry and physics, and such batteries are already commercially available and widely used in various portable systems (such as cameras, laptops, and cell phones). Developing advanced energy materials based on Li ion is an important step to meet the demands for low cost and environmentally friendly energy generation and storage systems [9]. Thus, hydrated lithium borates have attracted great attention recently. If the one-dimensional (1D) alkali borates, such as tubes, wires, rods, belts and whiskers, can be controllably synthesized, then similar to other typical 1D nanomaterials (such as carbon nanotubes [10–13], Si [14], LiFePO_4 [15], LiMn_2O_4 [16] nanowires), some novel properties and applications will be explored.

Controllable synthesis of lithium borates or lithium borate hydroxide is the first step to explore their properties and potential applications. In contrast with some conventional strategies for 1D borate synthesis, such as chemical vapor deposition and molten salt synthesis, hydrothermal process has been of much concern. Byrappa et al. reported $\text{Li}_3\text{B}_5\text{O}_8(\text{OH})_2$ hydrothermally synthesized in the system $\text{Li}_2\text{O}-\text{B}_2\text{O}_3-\text{H}_2\text{O}$ under low pressure–temperature conditions ($P < 100$ atm, $T = 240$ °C) for 7-day growth [1]. The as-synthesized $\text{Li}_3\text{B}_5\text{O}_8(\text{OH})_2$ was identified to be a

perspective superionic conductor material at about 523 K [17]. In addition, a new lithium borate as the enantiomer of the known tetragonal $\text{Li}_3\text{B}_5\text{O}_8(\text{OH})_2$ (PDF No. 44-0249) was reported by Li and Liu [18], using Li_2CO_3 and H_3BO_3 as the raw materials in the presence of pyridine and La_2O_3 . Up to now, only the structure and synthetic procedure of $\text{Li}_3\text{B}_5\text{O}_8(\text{OH})_2$ can be available in literatures [1,3,17,18], while the morphologies and their modulation are not revealed. What's more, $\text{Li}_3\text{B}_5\text{O}_8(\text{OH})_2$ is a very good precursor to obtain lithium borates.

The idea to hydrothermal synthesis of $\text{Li}_3\text{B}_5\text{O}_8(\text{OH})_2$ first and subsequently thermal conversion into $\text{Li}_2\text{B}_4\text{O}_7$ was explored to obtain high crystallinity $\text{Li}_2\text{B}_4\text{O}_7$ with potential application in Li-ion battery. The influences of process parameters, such as temperature, reaction time, and additives on the hydrothermal products, were investigated to controllable synthesis of high crystallinity orthorhombic $\text{Li}_3\text{B}_5\text{O}_8(\text{OH})_2$ (PDF No. 76-1956) micro-rods and/or tetragonal $\text{Li}_3\text{B}_5\text{O}_8(\text{OH})_2$ (PDF No. 72-1914) powders. The flux agent of NaCl was employed to assist the thermal decomposition of orthorhombic $\text{Li}_3\text{B}_5\text{O}_8(\text{OH})_2$, leading to pore-free $\text{Li}_2\text{B}_4\text{O}_7$ with quasi polyhedron morphology.

2. Experimental

2.1. Hydrothermal synthesis of lithium borate hydroxides

All of the reactants were of analytical grade without further purification. In a typical procedure, 3.4160 g of $\text{LiOH}(\text{s})$ and 1.1749 g of $\text{H}_3\text{BO}_3(\text{s})$ were mixed with 24 mL of deionized (DI) water (molar ratio: $\text{Li}:\text{B} = 1:2$, $[\text{Li}^+] = 1.17$ mol L^{-1}), leading to a white slurry which was supplemented with a specific additive (polyvinylpyrrolidone (PVP), ethylene diamine tetraacetic acid (EDTA), or hexadecyl trimethyl ammonium bromide (CTAB)). The mass ratio of the additive to the

* Corresponding authors. Tel.: +86 537 4456301; fax: +86 537 4456305.

E-mail addresses: zhuwancheng@tsinghua.org.cn (W. Zhu), zhang-qiang@mails.tsinghua.edu.cn (Q. Zhang).

theoretical product was 2.5 wt.%. While for CTAB, the amount of the additive was altered within the range of 0–15.0 wt.% to evaluate the corresponding effect on the hydrothermal product. Then the as-prepared slurry was transferred into a Teflon lined stainless steel autoclave with a capacity of 60 mL. The autoclave was sealed and heated to 150–210 °C (heating rate: 2 °C min⁻¹) and kept under an isothermal condition for 6.0–24.0 h, and then cooled down to room temperature naturally. The products were filtered, washed with DI water and absolute alcohol, and finally dried in vacuum at 90 °C for 12.0 h.

2.2. Thermal conversion of lithium borate hydroxides into lithium borates

The Li₃B₅O₈(OH)₂ (orthorhombic) powder was moved to a porcelain boat located in a horizontal furnace, which was heated to 500–700 °C (heating rate: 2 °C min⁻¹) and kept in an isothermal state for 2.0 h. After calcination, the product was cooled down to room temperature. When calcination was carried out in the presence of NaCl saturated solution, the as-obtained product was washed with DI water to remove residual NaCl, and dried at 90 °C for 12.0 h for further characterization.

2.3. Characterization

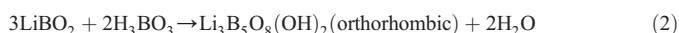
The composition and structure of the samples were identified by an X-ray powder diffractometer (XRD, D8-Advance, Bruker, Germany) using Cu K_α radiation (λ = 1.5406 Å). The morphology of the samples was examined with a field emission scanning electron microscopy (SEM, JSM 7401F, JEOL, Japan) and a high resolution transmission electron microscopy (TEM, JEM-2010, JEOL, Japan). The thermal decomposition behavior of the sample was detected by a simultaneous

thermal analyzer (NETZSCH STA 409 PC/PG, Germany) from 30 to 900 °C, carried out in dynamic air with a heating rate of 10.0 °C min⁻¹.

3. Results and discussion

3.1. Hydrothermal synthesis of lithium borate hydroxides

Fig. 1 shows the morphology evolution of the Li₃B₅O₈(OH)₂ products during hydrothermal synthesis. The orthorhombic Li₃B₅O₈(OH)₂ (Fig. 1(a₁–a₃)) micro-rods (Fig. 1(b–d)) were obtained at 150 °C for 6.0–24.0 h, in the absence of any additive. The related chemical reactions involved in the hydrothermal processes were written as follows [1]:



With the elongation of the reaction time from 6.0 to 12.0 h, the diffraction peaks became sharper (Fig. 1(a₂)), indicating the crystallinity of product turned higher. All of the diffraction peaks were readily indexed as those of the standard orthorhombic Li₃B₅O₈(OH)₂ (PDF No. 76-1956). When the hydrothermal growth prolonged to 24.0 h (Fig. 1(a₃)), the crystallinity tended to decrease, and uniform micro-rods with smooth surfaces (Fig. 1(c)) evolved into nonuniform micro-rods with relatively rough surfaces (Fig. 1(d)). In accordance with the XRD results (Fig. 1(a₂–a₃)), this morphology evolution reconfirmed the degradation of the product crystallinity when hydrothermally treated overtime. Consequently, to obtain Li₃B₅O₈(OH)₂ with uniform morphology, the hydrothermal time hereafter was set as 12.0 h.

The influence of the hydrothermal temperature on the composition and the morphology of the products are illustrated in Fig. 2.

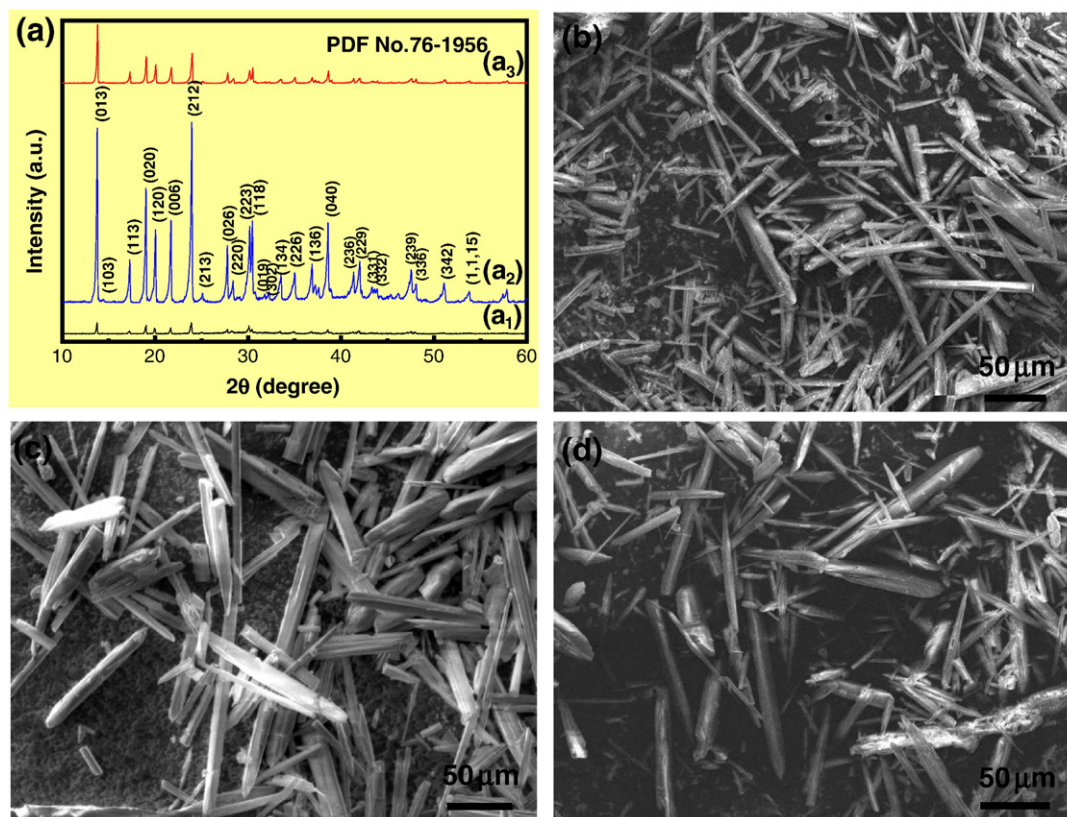


Fig. 1. XRD patterns (a) and morphologies (b–d) of the as-grown products derived at 150 °C for 6.0 (a₁, b), 12.0 (a₂, c), and 24.0 (a₃, d) h.

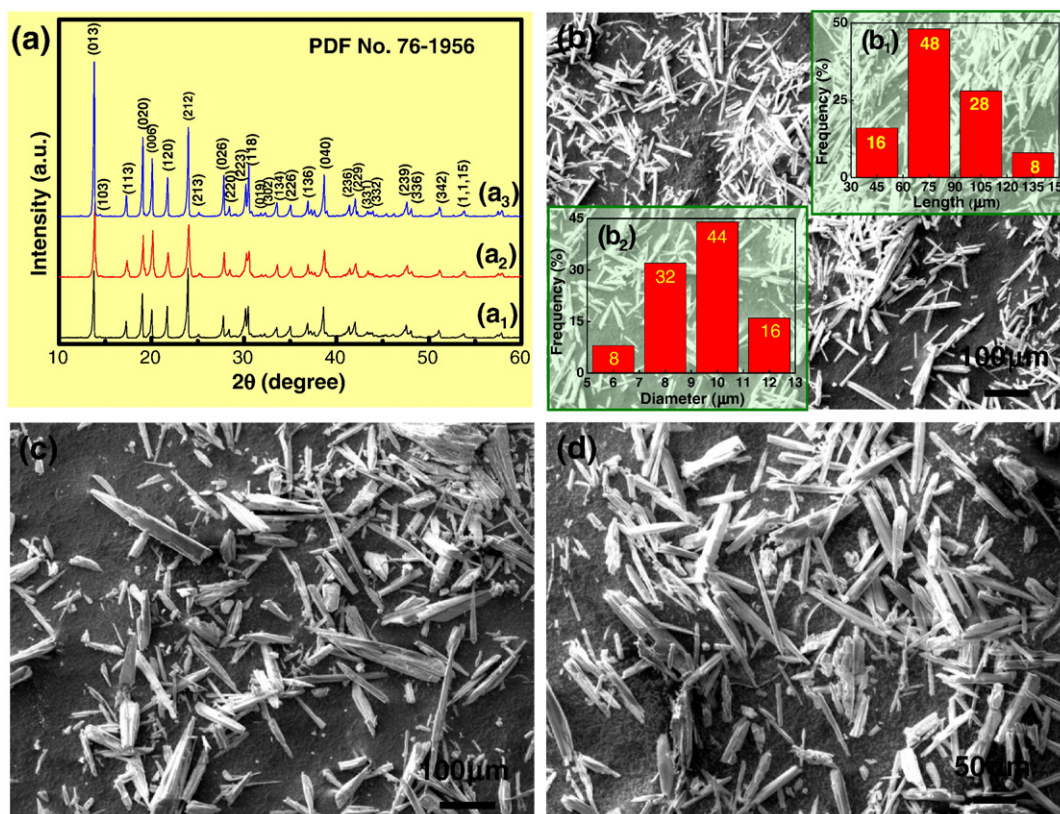


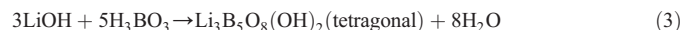
Fig. 2. XRD patterns (a) and morphologies (b–d) of the as-grown products derived from 12.0 h hydrothermal growth at 150 (a₁, b), 180 (a₂, c), and 210 (a₃, d) °C. The insert figure illustrates the length (b₁) and diameter distribution (b₂) of the as-grown products.

Orthorhombic Li₃B₅O₈(OH)₂ (Fig. 2(a₁–a₃)) micro-rods (Fig. 2(b–d)) were obtained when the hydrothermal synthesis was operated at a temperature of 150–210 °C. XRD patterns (Fig. 2(a₁–a₃)) illustrated that all of the samples were composed of the orthorhombic Li₃B₅O₈(OH)₂ (PDF No. 76-1956). A higher hydrothermal temperature was favorable for the formation of Li₃B₅O₈(OH)₂ with a higher crystallinity. Nevertheless, thicker micro-rods with distinctly broad size distribution were obtained at a temperature of 180–210 °C (Fig. 2(c–d)). In contrast, relatively low temperature of 150 °C favored the formation of micro-rods with uniform 1D morphology, 76% of which had a length of 60–120 μm (Fig. 2(b₁)) and a diameter of 7–11 μm (Fig. 2(b₂)).

Surface-capping agents, such as PVP [19], EDTA [20–22], and CTAB [23–26], have been widely used for the synthesis of the 1D nanostructure. To obtain 1D Li₃B₅O₈(OH)₂ with higher aspect ratio, various additives, such as PVP, EDTA, and CTAB, were individually added. With the mass ratio of the additive to the theoretical product as 2.5%, PVP, EDTA, and CTAB all favored the formation of the orthorhombic Li₃B₅O₈(OH)₂ (PDF No. 76-1956) (Fig. 3(a₁–a₃)). Comparatively, with the additive altered from PVP to EDTA to CTAB, the product crystallinity became higher. Meanwhile, the addition of PVP led to low aspect ratio rod-like Li₃B₅O₈(OH)₂ structure with rough surface (Fig. 3(b)), whereas the introduction of EDTA resulted in relatively high aspect ratio rod-like Li₃B₅O₈(OH)₂ structure with smooth surface (Fig. 3(c)). In contrast, CTAB brought uniform rod-like Li₃B₅O₈(OH)₂ structure with smooth surface (Fig. 3(d, d₁)) and a length of 20–60 μm, and 65% of the rods had an aspect ratio of 4–16 (Fig. 3(d₂)). This is higher than the aspect ratio of those obtained without any additive (Figs. 1 and 2). As for the formation mechanism of the orthorhombic Li₃B₅O₈(OH)₂ micro-rods, it is connected with the specific anisotropic crystal structure of the orthorhombic Li₃B₅O₈(OH)₂, taking into consideration that the micro-rods with a relatively low aspect ratio are formed without any additives. This is quite similar to the hydrothermal formation of MgBO₂(OH) nanowhiskers [27,28]

and nanowires [29]. It is known that, CTAB is a cationic surfactant with a critical micelle concentration (CMC) of 0.03% (0.9–1.0 mM) [30]. Above the CMC, rod-like micelles occurred (rather than spherical ones), and the size of micelles became larger with the concentration of CTAB increasing, leading to long and flexible worm-like micelles [31]. Thus, in our case, CTAB could easily form rod-like micelles, which served as a soft template [32] and finally promoted the oriented growth of orthorhombic Li₃B₅O₈(OH)₂ micro-rods with a high aspect ratio.

However, when the mass ratio of CTAB to product was increased to 10.0–15.0%, the hydrothermal products changed into pure phase tetragonal Li₃B₅O₈(OH)₂ (PDF No. 72-1914, Fig. 3(a₄)) of irregular shape (Fig. 3(e)), rather than rod-like orthorhombic Li₃B₅O₈(OH)₂ phase. The overall chemical reaction involved in the hydrothermal conversion thus was illustrated as follows:



Compared with the tetragonal Li₃B₅O₈(OH)₂ phase (PDF No. 44-0249) hydrothermally synthesized at 170 °C for 3 days by using the Li₂B₄O₇·3H₂O and H₃BO₃ as the raw materials in the presence of pyridine [18], the Li₃B₅O₈(OH)₂ with orthorhombic (PDF No. 76-1956) and tetragonal (PDF No. 72-1914) phase were easily obtained via tuning the amount of CTAB addition. A low amount of the additive (2.5% of the product) was favorable for the formation of rod-like orthorhombic Li₃B₅O₈(OH)₂ (PDF No. 76-1956), and a relatively high mass ratio of the additive to product of 10.0–15.0% was favorable for the formation of irregular tetragonal Li₃B₅O₈(OH)₂ (PDF No. 72-1914). In contrast with the reported tetragonal Li₃B₅O₈(OH)₂ phase (PDF No. 44-0249) [18], the present tetragonal Li₃B₅O₈(OH)₂ (PDF No. 72-1914) exhibited significant reflection peaks at 2θ of 14.28°, and also within the range of 63.5–89.4°. Thus, the present tetragonal Li₃B₅O₈(OH)₂ was indexed to the PDF card No. 72-1914.

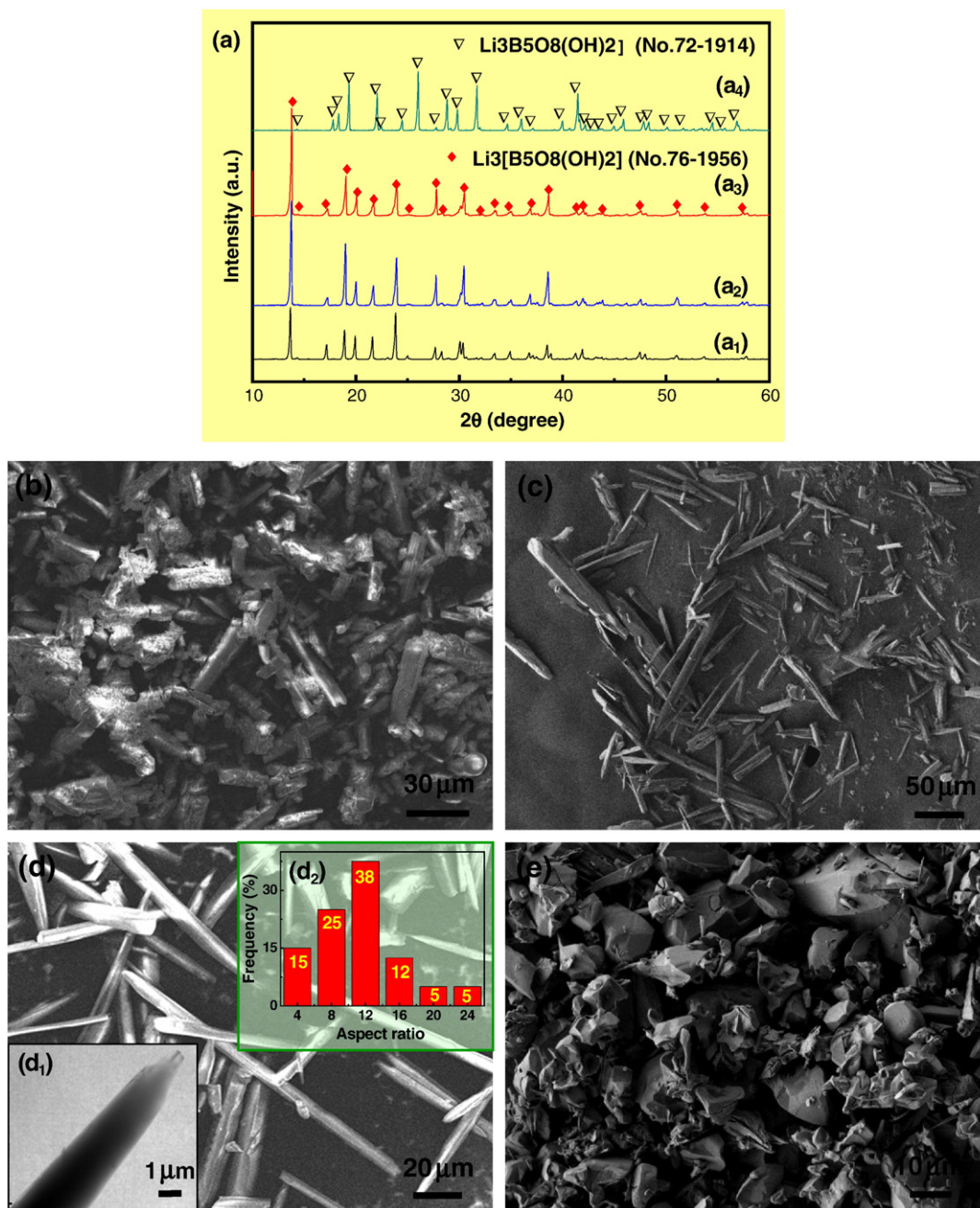


Fig. 3. XRD patterns (a) and morphologies (b–e) of the as-grown products derived in the presence of the various additives. Molar ratio: Li:B = 1:2; temperature (°C): 150; reaction time (h): 12.0; (a₁, b)-PVP, (a₂, c)-EDTA, (a₃, a₄, d, e)-CTAB, mass ratio of the additive to the theoretical product = 2.5% (a₁–a₃, b–d), 10.0% (a₄, e); (d₁) TEM image of the product with CTAB as additive; (d₂) Aspect ratio distribution of the product with CTAB as additive. ♦: Li₃B₅O₈(OH)₂ (orthorhombic, PDF No.76-1956). ▽: Li₃B₅O₈(OH)₂ (tetragonal, PDF No.72-1914).

3.2. Thermal conversion of lithium borate hydroxides into lithium borates

To obtain the thermal decomposition behavior of Li₃B₅O₈(OH)₂, TG–DSC curves of the orthorhombic Li₃B₅O₈(OH)₂ hydrothermally synthesized at 150 °C for 12.0 h (in the absence of any additive) are shown in Fig. 4. The mass of the sample decreased at a very slow rate when the temperature was below 450 °C. This indicated the exceptional high dehydration temperature of the hydrothermal product. The mass of the sample went down at a very fast rate within the temperature range of 450–500 °C due to the dehydration process, and kept almost constant at the temperature above 600 °C. The mass loss of the sample between 450 and 600 °C was *ca.* 8.2%, by and large

in accordance with the theoretical mass loss (7.6%) for the thermal decomposition of Li₃B₅O₈(OH)₂ [4,33]:



Simultaneously, the DSC curve showed a sharp endothermic peak at 475.9 °C, owing to the dehydration of the hydrothermally synthesized orthorhombic Li₃B₅O₈(OH)₂ (PDF No. 76-1956) within a temperature range of 420–500 °C. This was lower than that of the reported tetragonal Li₃B₅O₈(OH)₂ (PDF No. 44-0249) [18]. Additionally, there was also an exothermic peak at 853.8 °C, probably due to the recrystallization of the calcined product, which was similar to the characteristics of other borates reported in literature [34].

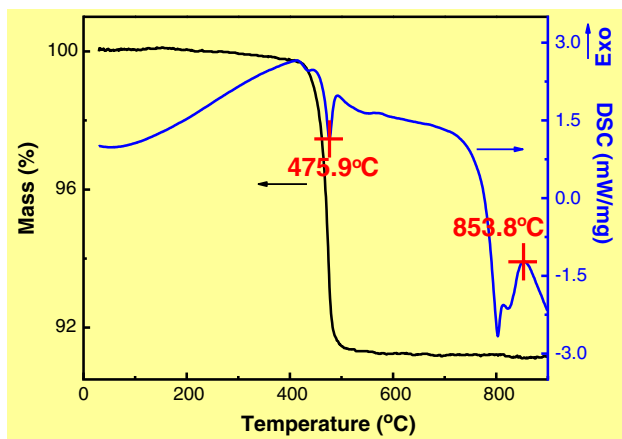


Fig. 4. TG–DSC curves of the orthorhombic $\text{Li}_3\text{B}_5\text{O}_8(\text{OH})_2$ hydrothermally synthesized in the absence of any additive.

The orthorhombic $\text{Li}_3\text{B}_5\text{O}_8(\text{OH})_2$ (Fig. 5(a₁, b)) was used as the precursor for the thermal conversion into lithium borates. The orthorhombic $\text{Li}_3\text{B}_5\text{O}_8(\text{OH})_2$ were calcined at 500 (Fig. 5(a₂, c)) and 600 °C (Fig. 5(a₃, d)). The calcination at 500 °C for 2.0 h in air led to a mixture with irregular shapes (Fig. 5(a₂, c)), and the mixture was subsequently convinced as $\text{Li}_2\text{B}_4\text{O}_7$ (PDF No. 79-0963) and monoclinic LiBO_2 (PDF No. 84-0118, i.e. $\alpha\text{-LiBO}_2$) derived from a high temperature calcination at 600 °C for 2.0 h (Fig. 5(a₃, d)). Apparently, the phase conversion during the calcination of orthorhombic $\text{Li}_3\text{B}_5\text{O}_8(\text{OH})_2$

reconfirmed the chemical reaction in the course of the thermal decomposition (450–600 °C) demonstrated in Eq. (4), and also in well agreement with the reference [4]. In addition, compared to that of $\alpha\text{-LiBO}_2$ in the XRD pattern obtained at 600 °C (Fig. 5(a₃)), the relative intensity of the diffraction peaks of $\text{Li}_2\text{B}_4\text{O}_7$ (PDF No. 79-0963) was higher than that obtained at 500 °C (Fig. 5(a₂)). This revealed that the relative content of $\alpha\text{-LiBO}_2$ (PDF No. 84-0118) in the mixed calcined product decreased with the calcination temperature increasing. Meanwhile, the calcined product acquired at 600 °C (Fig. 5(a₃)) exhibited a relatively higher crystallinity compared with that obtained at 500 °C (Fig. 5(a₂)). Nevertheless, the TEM observation (Fig. 5(d₁)) definitely showed that, the calcined product obtained at 600 °C containing multitude of mesopores within the bulk phase due to the former dehydration. The generation of pores was quite analogous to the dehydration phenomenon during the thermal conversion from $\text{MgBO}_2(\text{OH})$ nanowhiskers to $\text{Mg}_2\text{B}_2\text{O}_5$ nanowhiskers [34].

Our previous work has indicated that, a high calcination temperature favors the formation of high crystallinity product [34], and the flux agent (such as NaCl) promotes the formation of pore-free high crystallinity nanostructures [35]. Thus, higher calcination temperature as 700 °C and NaCl were employed for the calcination of orthorhombic $\text{Li}_3\text{B}_5\text{O}_8(\text{OH})_2$, as shown in Fig. 6. After the calcination (700 °C, 2.0 h) of the previously synthesized hydrothermal product (Fig. 5(a₁, b)) in the presence of the saturated NaCl solution, $\text{Li}_2\text{B}_4\text{O}_7$ (PDF No. 79-0963, Fig. 6(a)) particles with uniform quasi polyhedron morphology (Fig. 6(b)) were obtained. Obviously, the flux-assisted thermal conversion of orthorhombic $\text{Li}_3\text{B}_5\text{O}_8(\text{OH})_2$ has successfully led to the formation of pore-free high crystallinity $\text{Li}_2\text{B}_4\text{O}_7$. Similar to the formation of $\text{Mg}_2\text{B}_2\text{O}_5$ nanowhiskers [35], the flux agent NaCl also

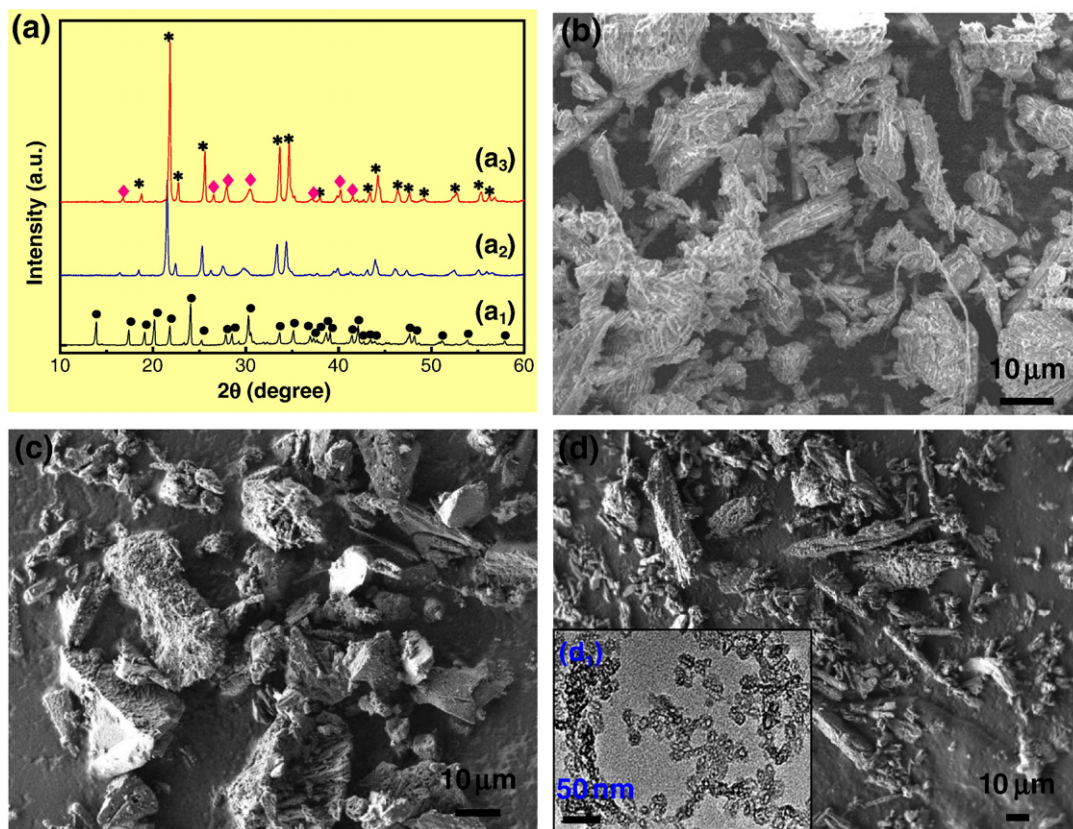


Fig. 5. XRD patterns (a) and morphologies (b–d, d₁) of the orthorhombic $\text{Li}_3\text{B}_5\text{O}_8(\text{OH})_2$ (a₁, b) and corresponding calcined products (a₂–a₃, c–d, d₁) treated at various temperatures. Hydrothermal condition: 150 °C, 12.0 h (a₁, b). Calcination condition: heating rate (°C min⁻¹): 2.0; time (h): 2.0; temperature (°C): (a₂, c)–500, (a₃, d, d₁)–600. ●: $\text{Li}_3\text{B}_5\text{O}_8(\text{OH})_2$ (orthorhombic), *: $\text{Li}_2(\text{B}_4\text{O}_7)$ (PDF No. 79-0963), ◆: LiBO_2 (PDF No. 84-0118).

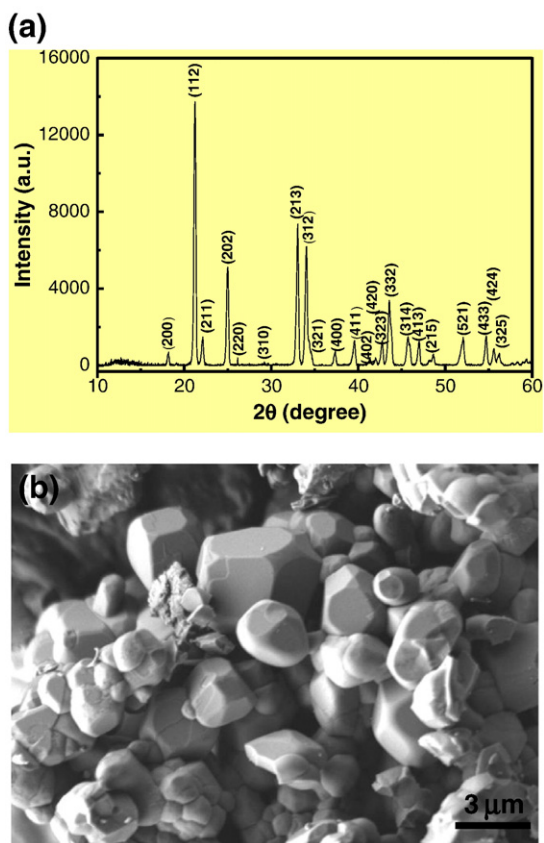


Fig. 6. XRD patterns (a) and morphologies (b) of the product $\text{Li}_2(\text{B}_4\text{O}_7)$ (PDF No.79-0963) calcined at 700 °C for 2.0 h, in the presence of the saturated NaCl solution.

has been served as the requisite liquid medium for the rearrangement of the porous $\text{Li}_2\text{B}_4\text{O}_7$ phase and finally promoted the formation of the pore-free $\text{Li}_2\text{B}_4\text{O}_7$ structures.

4. Conclusions

By using $\text{LiOH}\cdot\text{H}_2\text{O}$ and H_3BO_3 as the reactants, uniform high crystallinity orthorhombic $\text{Li}_3\text{B}_5\text{O}_8(\text{OH})_2$ (PDF No. 76-1956) micro-rods (length: 20–60 μm , aspect ratio: 6–14) and tetragonal $\text{Li}_3\text{B}_5\text{O}_8(\text{OH})_2$ (PDF No. 72-1914) particles with irregular shape were hydrothermally synthesized. The presence of the CTAB with a mass ratio of 2.5% promoted the oriented growth of the $\text{Li}_3\text{B}_5\text{O}_8(\text{OH})_2$ micro-rods. A high mass ratio of CTAB (10.0–15.0% to the theoretical product) was favorable for the formation of tetragonal $\text{Li}_3\text{B}_5\text{O}_8(\text{OH})_2$. The thermal decomposition of orthorhombic $\text{Li}_3\text{B}_5\text{O}_8(\text{OH})_2$ at 500–600 °C resulted in $\text{Li}_2\text{B}_4\text{O}_7$ and $\alpha\text{-LiBO}_2$, and the flux agent NaCl assisted high temperature (700 °C) calcination led to the pore-free high crystallinity $\text{Li}_2\text{B}_4\text{O}_7$ with quasi polyhedron morphology. The present work enlarged the controllable synthesis of the alkali borates, especially enriched the study on the lithium borates which can be

used as a perspective superionic conductor, and might also provide more options for the materials of the lithium ion batteries in the future.

Acknowledgements

This work was supported by the State Key Laboratory of Chemical Engineering, China (SKL-ChE-09A02), a Project of Shandong Province Higher Educational Science and Technology Program, China (J10LB15), the Excellent Middle-Aged and Young Scientist Award Foundation of Shandong Province, China (BS2010CL024), and the Youth Foundation of Qufu Normal University, China (XJ200926).

References

- [1] K. Byrappa, K.V.K. Shekar, S. Gali, *Cryst. Res. Technol.* 27 (1992) 767–772.
- [2] S.A. Guretskii, A.P. Ges, D.I. Zhigunov, A.A. Ignatenko, N.A. Kalanda, L.A. Kurnevich, A.M. Luginets, A.S. Milovanov, P.V. Molchan, *J. Cryst. Growth* 156 (1995) 410–412.
- [3] E. Betourne, M. Touboul, *J. Alloys Compd.* 255 (1997) 91–97.
- [4] M. Touboul, N. Penin, G. Nowogrocki, *Solid State Sci.* 5 (2003) 1327–1342.
- [5] Z.S. Hu, L.G. Wang, Z.W. Ou, L. Huang, R. Lai, T. He, J.X. Dong, G.X. Chen, *Powder Technol.* 114 (2001) 163–167.
- [6] W.C. Zhu, G.D. Li, Q. Zhang, L. Xiang, S.L. Zhu, *Powder Technol.* 203 (2010) 265–271.
- [7] P. Li, Z.H. Liu, *J. Chem. Eng. Data* 54 (2009) 830–832.
- [8] X.X. Shi, Y. Xiao, L.J. Yuan, J.T. Sun, *Powder Technol.* 189 (2009) 462–465.
- [9] D.S. Su, R. Schlogl, *ChemSusChem* 3 (2010) 136–168.
- [10] J.Q. Huang, Q. Zhang, F. Wei, W.Z. Qian, D.Z. Wang, L. Hu, *Carbon* 46 (2008) 291–296.
- [11] J.Q. Huang, Q. Zhang, M.Q. Zhao, F. Wei, *Nano Res.* 2 (2009) 872–881.
- [12] F. Wei, Q. Zhang, W.Z. Qian, H. Yu, Y. Wang, G.H. Luo, G.H. Xu, D.Z. Wang, *Powder Technol.* 183 (2008) 10–20.
- [13] J.Q. Huang, Q. Zhang, M.Q. Zhao, G.H. Xu, F. Wei, *Nanoscale* 2 (2010) 1401–1404.
- [14] M. Leisner, A. Cojocaru, E. Ossei-Wusu, J. Carstensen, H. Foll, *Nanoscale Res. Lett.* 5 (2010) 1502–1506.
- [15] E. Hosono, Y.G. Wang, N. Kida, M. Enomoto, N. Kojima, M. Okubo, H. Matsuda, Y. Saito, T. Kudo, I. Honma, H.S. Zhou, *ACS Appl. Mater. Interfaces* 2 (2010) 212–218.
- [16] E. Hosono, T. Kudo, I. Honma, H. Matsuda, H.S. Zhou, *Nano Lett.* 9 (2009) 1045–1051.
- [17] K. Byrappa, V.P. Jayantharaja, K.V.K. Shekar, V. Rajeev, V.J. Hanumesh, A.R. Kulkarni, A.B. Kulkarni, *J. Mater. Sci.* 32 (1997) 1599–1602.
- [18] P. Li, Z.H. Liu, *J. Chem. Eng. Data* 55 (2010) 2682–2686.
- [19] M. Giersig, I. Pastoriza-Santos, L.M. Liz-Marzan, *J. Mater. Chem.* 14 (2004) 607–610.
- [20] H.F. Chen, K. Sun, Z.Y. Tang, R.V. Law, J.F. Mansfield, A. Czajka-Jakubowska, B.H. Clarkson, *Cryst. Growth Des.* 6 (2006) 1504–1508.
- [21] C.W. Xu, H. Wang, P.K. Shen, S.P. Jiang, *Adv. Mater.* 19 (2007) 4256–4259.
- [22] X.T. Sun, W.T. Shi, L. Xiang, W.C. Zhu, *Nanoscale Res. Lett.* 3 (2008) 386–389.
- [23] N.R. Jana, L. Gearheart, C.J. Murphy, *Chem. Commun.* (2001) 617–618.
- [24] Y.K. Liu, D.D. Hou, G.H. Wang, *Chem. Phys. Lett.* 379 (2003) 67–73.
- [25] K.L. Lin, J. Chang, J.X. Lu, *Mater. Lett.* 60 (2006) 3007–3010.
- [26] R.S. Yadav, A.C. Pandey, *Struct. Chem.* 20 (2009) 847–850.
- [27] W.C. Zhu, L. Xiang, T.B. He, S.L. Zhu, *Chem. Lett.* 35 (2006) 1158–1159.
- [28] W.C. Zhu, S.L. Zhu, L. Xiang, *CrystEngComm* 11 (2009) 1910–1919.
- [29] W.C. Zhu, X.Y. Zhang, L. Xiang, S.L. Zhu, *Nanoscale Res. Lett.* 4 (2009) 724–731.
- [30] M. Delsanti, A. Moussaid, J.P. Munch, *J. Colloid Interface Sci.* 157 (1993) 285–290.
- [31] S.H. Han, W.G. Hou, W.X. Dang, J. Xu, J.F. Hu, D.Q. Li, *Mater. Lett.* 57 (2003) 4520–4524.
- [32] F.C. Meldrum, N.A. Kotov, J.H. Fendler, *J. Phys. Chem.* 98 (1994) 4506–4510.
- [33] M. Touboul, E. Betourne, *Solid State Ionics* 84 (1996) 189–197.
- [34] W.C. Zhu, L. Xiang, Q. Zhang, X.Y. Zhang, L. Hu, S.L. Zhu, *J. Cryst. Growth* 310 (2008) 4262–4267.
- [35] W.C. Zhu, Q. Zhang, L. Xiang, F. Wei, X.T. Sun, X.L. Piao, S.L. Zhu, *Cryst. Growth Des.* 8 (2008) 2938–2945.